Letters

Power Characterization of Isolated Bidirectional Dual-Active-Bridge DC–DC Converter With Dual-Phase-Shift Control

Biao Zhao, Qiang Song, and Wenhua Liu

***Abstract*—Compared to the traditional single-phase-shift control, dual-phase-shift (DPS) control can greatly improve the performance of the isolated bidirectional dual-active-bridge dc–dc converter (IBDC). This letter points out some wrong knowledge about transmission power of IBDC under DPS control in the earlier studies. On this basis, this letter gives the detailed theoretical and experimental analyses of the transmission power of IBDC under DPS control. And the experimental results showed agreement with theoretical analysis.**

***Index Terms*—Bidirectional converter, dc–dc converter, dual active bridge, phase-shift control, transmission power.**

I. Introduction

THE power transfer capability is one of the most fundamental and significant evaluating factors of isolated bidirectional dual-active-bridge dc–dc converter (IBDC) [1]–[4]. In order to improve the performance of IBDC, various control algorithms are explored.

Single-phase-shift (SPS) control is the most widely used algorithm in IBDC, but it is essentially an active-power-centered control algorithm. It not only lacks flexibility in power regulation, but also brings additional stress to the devices used in the converter during steady-state operation [1]–[5].

In order to improve the performance of SPS control, Bai and coworkers proposed a dual-phase-shift (DPS) control algorithm aiming at eliminating reactive power and increasing system power capability [5], [6]. Compared to the traditional SPS control, the DPS control has many significant advantages, which can decrease peak current, limit inrush current, eliminate reactive power, increase system efficiency, and minimize the output capacitance. The DPS control also has generality, which extended out a family of improved phase-shift control methods of IBDC, such as an improved modulation strategy that allows operating IBDC under soft switching in the whole operating range [7], [8], and a composite modulation strategy to extend the soft-switching range down to zero-load condition, reduces rms and peak currents, and results in significant size reduction of the transformer [9]. Krismer and Kolar studied the application performance improvement of IBDC with DPS control [10], [11]. These studies are mainly focused on the solutions to decrease power losses and optimize efficiency of IBDC and are conducted for an existing hardware prototype of an IBDC for an automotive application. They are of important significance to the actual engineering of IBDC. However, the studies in [5] are based on simulation and theoretical analysis, and there are some errors in the theoretical derive formulas about transmission power, which results in the wrong conclusion obtained in [5] that the maximum output power is 4/3 times of the SPS control. In subsequent research papers [6]–[11], the detailed analysis of the transmission power under DPS control is still not involved, and the further experiments are also not conducted to validate the earlier theoretical analysis.

In this letter, the detailed theoretical and experimental analyses of the transmission power of IBDC under DPS control will be conducted to make the right conclusion.

Manuscript received November 25, 2011; revised February 3, 2012; accepted February 24, 2012. Date of current version May 15, 2012. This work was supported by the National Natural Science Foundation of China under Grant 51077076. Recommended for publication by Associate Editor C. C. Mi.

The authors are with the Department of Electrical Engineering, Tsinghua University, Beijing 100084, China (e-mail: b-zhao09@mails.tsinghua.edu.cn; songqiang@mails.tsinghua.edu.cn; liuwenh@mails.tsinghua.edu.cn).

Color versions of one or more of the figures in this paper are available online at http://ieeexplore.ieee.org.

Digital Object Identifier 10.1109/TPEL.2012.2189586

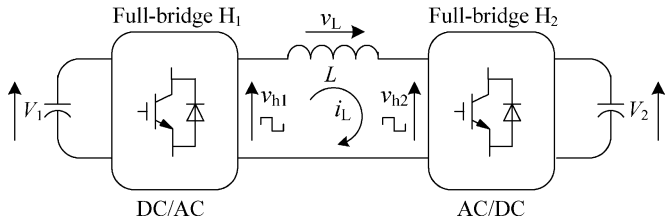

Fig. 1. Equivalent circuit of IBDC with phase-shift control.

II. Operation Principle of Dual-Phase-Shift Control

The equivalent circuit of IBDC with phase-shift control is shown in Fig. 1 [6]–[8], where V_1 and V_2 are input and output voltage, respectively, n is transformer voltage ratio, L is the sum of the transformer leakage inductance and auxiliary inductor, v_{h1} and v_{h2} are the equivalent ac output voltages of H_1 and H_2 in V_1 side, respectively, v_L and i_L are the voltage and current of inductor L, respectively.

The main waveforms of IBDC under DPS control with the conditions of $0 \le D_1 \le D_2 \le 1$ and $0 \le D_2 < D_1 \le 1$ are shown in Fig. 2, where T_{hs} is a half switching period, D_1 and D_2 are the inner and outer phase-shift ratio, respectively, where $0 \le D_1 \le 1$, $0 \le D_2 \le 1$ and $0 \le D_1 + D_2 \le 1$. Different from the SPS control, the DPS control adds another degree of freedom to the

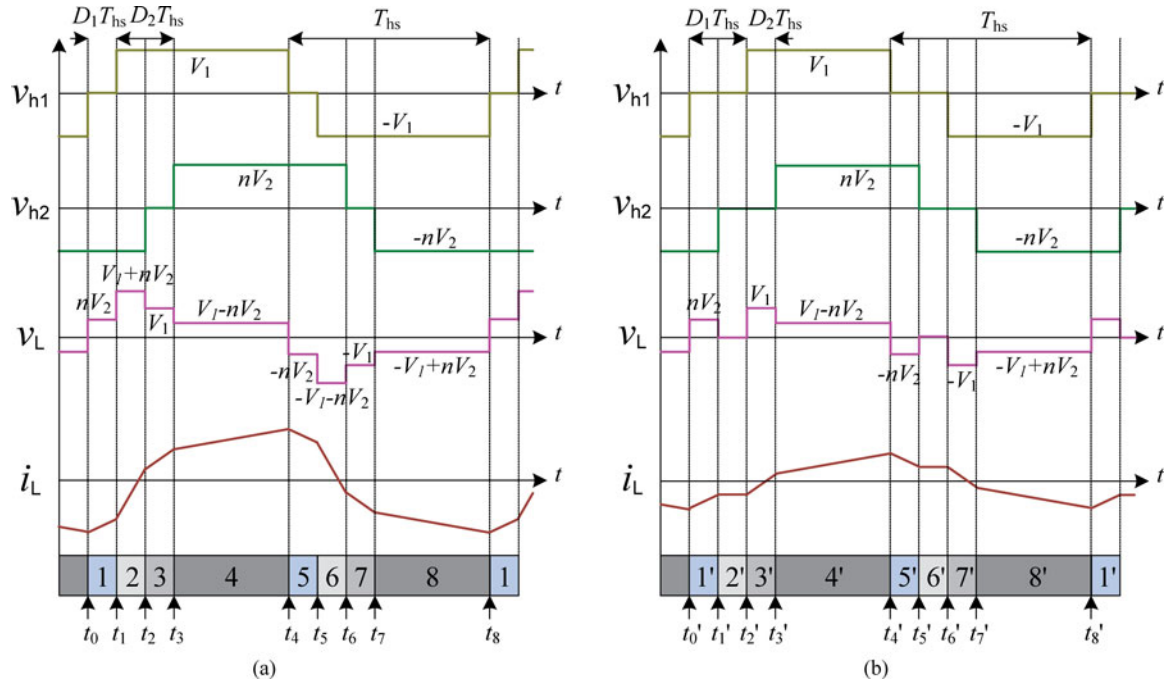

Fig. 2. (a) Waveforms of IBDC under DPS control in the condition of $0 \le D_1 \le D_2 \le 1$. (b) Waveforms of IBDC under DPS control in the condition of $0 \le D_2 < D_1 \le 1$.

TABLE I
TIMETABLE OF DPS CONTROL IN HALF SWITCHING CYCLE

$0 \le D_1 \le D_2 \le 1$ (DPS)		$0 \le D_2 < D_1 \le 1$ (DPS)	
Time	**Value**	**Time**	**Value**
t_0	0	t_0'	0
t_1	D_1T_{hs}	t_1'	D_2T_{hs}
t_2	D_2T_{hs}	t_2'	D_1T_{hs}
t_3	$(D_1+D_2)T_{hs}$	t_3'	$(D_1+D_2)T_{hs}$
t_4	T_{hs}	t_4'	T_{hs}

converter by adjusting the time sequence between the driving signals of diagonal semiconductor switches of bridges H_1 and H_2 in Fig. 1.

III. TRANSMISSION POWER OF IBDC WITH DPS CONTROL

From the equivalent circuit in Fig. 1, the expressions of i_L for each interval defined in Fig. 2 yields can be expressed as follows:

$$\frac{di_L(t)}{dt} = \frac{v_{h1}(t) - v_{h2}(t)}{L}. \tag{1}$$

Assuming that the initial time of one switching cycle is zero, the timetable can be shown in Table I. Considering the average current of the inductors over one switching period $2T_{hs}$ should be zero in the steady state, combining (1) and Table I, the peak currents of half switching cycle can be derived in Table II, where $f_s = 1/(2T_{hs})$ is the switching frequency, and $k = V_1/nV_2$ is the voltage conversion ratio.

From Fig. 2, the average transmission power of the IBDC converter with DPS control can be expressed as follows:

$$P = \frac{1}{T_{hs}} \int_0^{T_{hs}} v_{h1} i_L(t) dt. \tag{2}$$

Based on these expressions, the average transmission power of the IBDC with DPS and SPS control can be derived in Table III, where D is the phase-shift ratio of the SPS control.

IV. COMPARATIVE ANALYSIS OF POWER CHARACTERIZATION

For the convenience of analysis, the unified transmission power of the IBDC under DPS and SPS control are defined as follows:

$$\begin{cases} p = \dfrac{P}{P_N} = \begin{cases} 4D_2(1-D_2) - 2D_1^2 & 0 \le D_1 \le D_2 \le 1 \\ 4D_2\left(1 - D_1 - \dfrac{1}{2}D_2\right) & 0 \le D_2 < D_1 \le 1 \end{cases} \\ p_T = \dfrac{P_T}{P_N} = 4D(1-D) \quad 0 \le D \le 1 \end{cases} \tag{3}$$

where P_N is the maximum power of the IBDC with SPS control, that is

$$P_N = \frac{nV_1V_2}{8f_sL}. \tag{4}$$

When taking the outer phase-shift ratio D_2 in DPS control is equal to the phase-shift ratio D in SPS control, the 3-D curves of the unified transmission power p and p_T varied with D_1 and D_2 can be shown in Fig. 3(a). As can be seen from Fig. 3(a), when $D_1 = 0$, then $p = p_T$, and with different D_1, p will be different with p_T. In fact, taking the derivative value of (3), we can derive

$$\frac{dp}{dD_1} = \begin{cases} -4D_1 & 0 \le D_1 \le D_2 \le 1 \\ -4D_2 & 0 \le D_2 < D_1 \le 1. \end{cases} \tag{5}$$

TABLE II
PEAK CURRENT OF DPS CONTROL IN HALF SWITCHING CYCLE

$0 \le D_1 \le D_2 \le 1$ (DPS)		$0 \le D_2 < D_1 \le 1$ (DPS)	
i_L	Value	i_L	Value
$i_L(t_0)$	$-\frac{nV_2}{4f_sL}[k(1-D_1)+(D_1+2D_2-1)]$	$i_L(t_0')$	$-\frac{nV_2}{4f_sL}[k(1-D_1)+(D_1+2D_2-1)]$
$i_L(t_1)$	$-\frac{nV_2}{4f_sL}[k(1-D_1)+(2D_2-D_1-1)]$	$i_L(t_1')$	$-\frac{nV_2}{4f_sL}[k(1-D_1)+(D_1-1)]$
$i_L(t_2)$	$-\frac{nV_2}{4f_sL}[k(D_1-2D_2+1)+(D_1-1)]$	$i_L(t_2')$	$-\frac{nV_2}{4f_sL}[k(1-D_1)+(D_1-1)]$
$i_L(t_3)$	$-\frac{nV_2}{4f_sL}[k(-D_1-2D_2+1)+(D_1-1)]$	$i_L(t_3')$	$-\frac{nV_2}{4f_sL}[k(-D_1-2D_2+1)+(D_1-1)]$

TABLE III
TRANSMISSION POWER OF DPS AND SPS CONTROL

Condition	P
$0 \le D_1 \le D_2 \le 1$ (DPS)	$\frac{nV_1V_2}{2f_sL}[D_2(1-D_2)-\frac{1}{2}D_1^2]$
$0 \le D_2 < D_1 \le 1$ (DPS)	$\frac{nV_1V_2}{2f_sL}D_2(1-D_1-\frac{1}{2}D_2)$
$0 \le D \le 1$ (SPS)	$\frac{nV_1V_2}{2f_sL}D(1-D)$

Combining (4) and considering the constraint $0 \le D_1 + D_2 \le 1$, we can derive

$$p_{\max} = \begin{cases} 4D_2(1-D_2) & D_1 = 0 \\ 2D_2(2-3D_2) & D_1 = D_2 \end{cases} \tag{6}$$

$$p_{\min} = \begin{cases} 2D_2(2-3D_2) & D_1 = D_2 \\ 2D_2^2 & D_1 = 1-D_2 \end{cases} \tag{7}$$

where $0 \le D_2 < 0.5$.

$$p_{\max} = \begin{cases} 4D_2(1-D_2) & D_1 = 0 \\ -- \end{cases} \tag{8}$$

$$p_{\min} = \begin{cases} 2(1-D_2)(3D_2-1) & D_1 = 1-D_2 \\ -- \end{cases} \tag{9}$$

where $0.5 \le D_2 \le 1$.

From (6) to (9), Fig. 3(a) can be converted to the 2-D picture, as shown in Fig. 3(b). The thickened line is the regulating curve of transmission power in SPS control, and the dark-shaded area is the regulating area of transmission power in DPS control. From Fig. 3(b), due to the addition of D_1, the regulating range of transmission power is changed from the single curve to the 2-D area. And with the same outer phase-shift ratio ($D_2 = D$), the DPS control offers wider power transmission range than the SPS control does, which will also enhance regulating flexibility. But the two control methods have the same global maximum power. This is not the conclusion obtained in [5] that the maximum output power is 4/3 times of the SPS control.

V. EXPERIMENTAL ANALYSIS

In order to verify the aforementioned theoretical analysis, a laboratory prototype is constructed based on TMS320F2812 DSP. And the main parameters of converter are as follows: auxiliary inductor $L_1 = 0.2$ mH, dc capacitors $C_1 = C_2 = 2200\ \mu$F, transformer voltage ratio $n = 2$, and switching frequency $f_s = 10$ kHz.

Fig. 4 shows the steady-state experimental waveforms of v_{h1}, v_{h2}, and i_L under SPS ($D_1 = 0$) and DPS ($D_1 = 0.4$) control for the same transmission power 380 W, where the output voltage is in closed-loop control for 48 V. From Fig. 4, the current stress is different in SPS and DPS control for the same transmission power, and the DPS control generates less current stress than the SPS control does. In other words, with the same current stress, the DPS control can transfer more power than the SPS control does.

Fig. 5 shows the curves of the transmission power varied with D_1 and D_2. The input voltage and the output load are specified as 220 V and 6 Ω, respectively. It can be seen that the transmission power of IBDC can be regulated both by D_1 and D_2 under DPS control. From Fig. 5(a), with the specified $D_1 \le D_2$, the IBDC obtains the similar transmission power at D_2 and $1 - D_2$, which coincides with the theoretical analysis in (4). From Fig. 5(b), the maximum and minimum values of transmission power in the condition of $0 \le D_1 \le D_2 \le 1$ are obtained about at $D_1 = 0$ and $D_1 = D_2$, in the condition of $0 \le D_2 < D_1 \le 1$ are obtained about at $D_1 = D_2$ and $D_1 = 1 - D_2$, and in the whole range are obtained about at $D_1 = 0$ and $D_1 = 1 - D_2$, respectively. And with the same outer phase-shift ratio D_2, the DPS control ($D_1 \ne 0$) can offer wider power transmission range than the SPS control ($D_1 = 0$) does that will also enhance regulating flexibility. But the two control methods have the approximately same global maximum power, which agrees with the aforementioned theoretical analysis in Section IV.

Fig. 6 shows the comparative 3-D curves of experimental and theoretical results of the transmission power varied with D_1

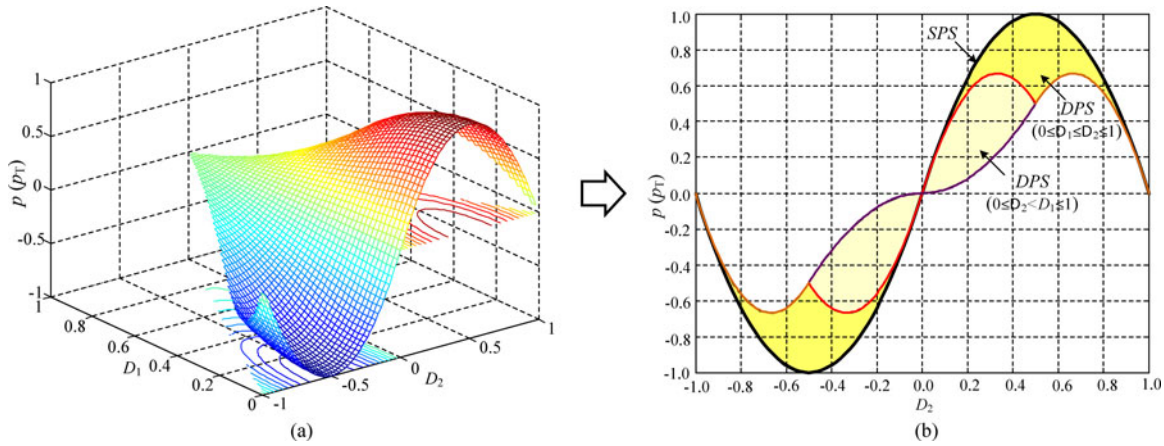

Fig. 3. Relation curves of the unified transmission power p (p_T) with D_1 and D_2. (a) 3-D curves. (b) 2-D curves.

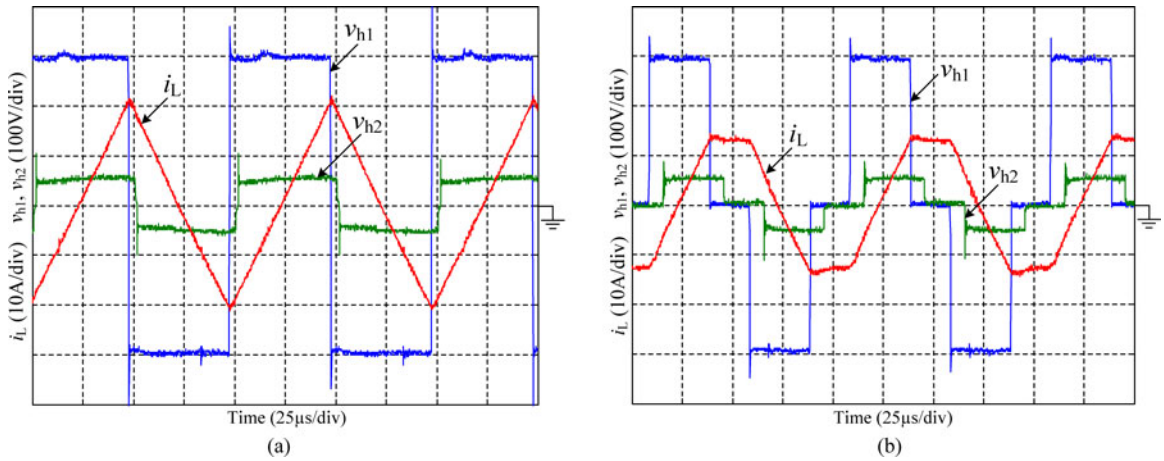

Fig. 4. Experimental waveforms of v_{h1}, v_{h2}, and i_L under SPS and DPS control for the same transmission. (a) SPS control with $V_1 = 300$ V, and $V_2 = 48$ V. (b) DPS control with $V_1 = 300$ V, $V_2 = 48$ V, and $D_1 = 0.4$.

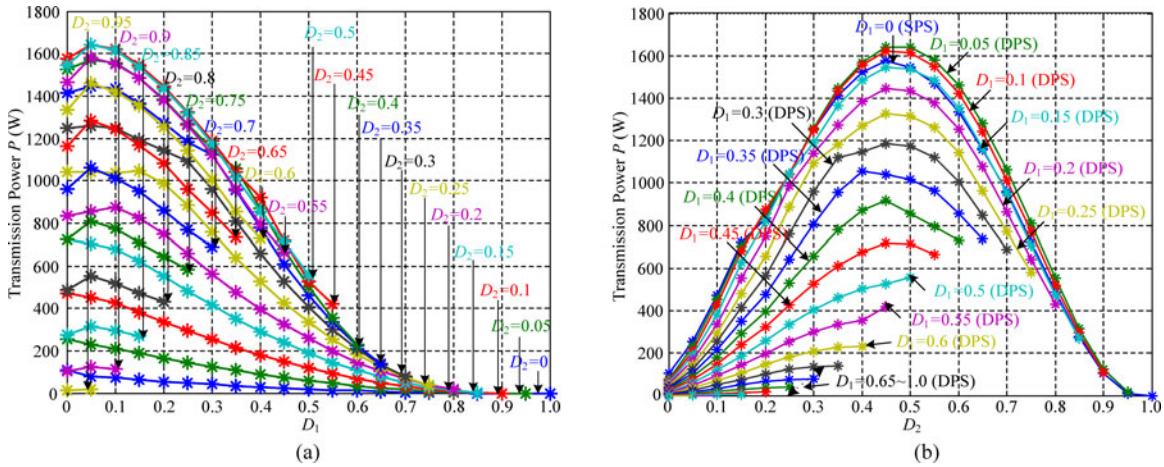

Fig. 5. Curves of the transmission power varied with D_1 and D_2. (a) Curves of the transmission power varied with D_1 when D_2 is specified. (b) Curves of the transmission power varied with D_2 when D_1 is specified.

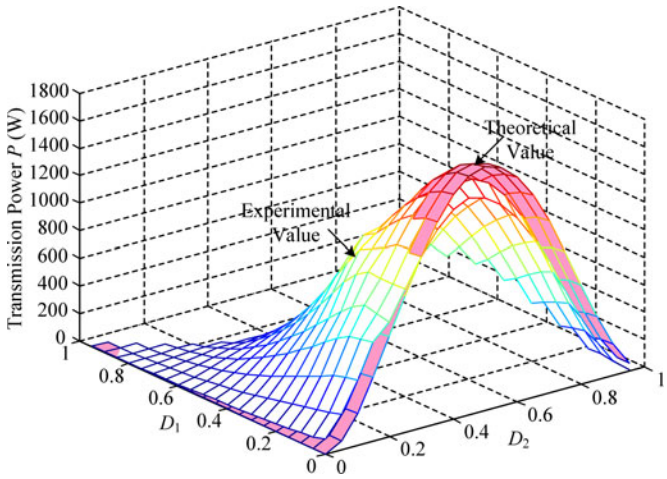

Fig. 6. Comparative 3-D curves of experimental and theoretical results of the transmission power varied with D_1 and D_2.

and D_2. As can be seen from Fig. 6, the experimental results basically coincide with the theoretical analysis across the whole range.

VI. Conclusion

In this letter, the detailed theoretical and experimental analyses of the transmission power of IBDC under DPS control have been conducted. And the experimental results showed agreement with theoretical analysis. Some conclusions can be found from the study: with the same outer phase-shift ratio D_2, the DPS control can offer wider power transmission range than the SPS control does that will also enhance regulating flexibility, and with the same current stress, the DPS control can transfer more power than the SPS control does; however, the two control methods have the same global maximum power, which is not the conclusion obtained in [5] that the maximum output power is 4/3 times of the SPS control.

References

[1] I. Shigenori and A. Hirofumi, "A bidirectional isolated DC-DC converter as a core circuit of the next-generation medium-voltage power conversion system," *IEEE Trans. Power Electron.*, vol. 22, no. 2, pp. 535–542, Mar. 2007.

[2] J. Shi, W. Gou, H. Yuan, T. Zhao, and A. Q. Huang, "Research on voltage and power balance control for cascaded modular solid-state transformer," *IEEE Trans. Power Electron.*, vol. 26, no. 4, pp. 1154–1167, Apr. 2011.

[3] Y. H. Xie, J. Sun, and S. F. James, "Power flow characterization of a bidirectional galvanically isolated high-power DC/DC converter over a wide operating range," *IEEE Trans. Power Electron.*, vol. 25, no. 1, pp. 54–65, Jan. 2010.

[4] H. Bai, C. Mi, and S. Gargies, "The short-time-scale transient processes in high-voltage and high-power isolated bidirectional dc-dc converters," *IEEE Trans. Power Electron.*, vol. 23, no. 6, pp. 2648–2656, Nov. 2008.

[5] H. Bai and C. Mi, "Eliminate reactive power and increase system efficiency of isolated bidirectional dual-active-bridge DC-DC converters using novel dual-phase-shift control," *IEEE Trans. Power Electron.*, vol. 23, no. 6, pp. 2905–2914, Nov. 2008.

[6] H. Bai, Z. Nie, and C. Mi, "Experimental comparision of traditional phase-shift, dual-phase-shift, and model-based control of isolated bidirectional dc-dc converters," *IEEE Trans. Power Electron.*, vol. 25, no. 6, pp. 1444–1449, Jun. 2010.

[7] G. G. Oggier, G. O. García, and A. R. Oliva, "Modulation strategy to operate the dual active bridge dc-dc converter under soft switching in the whole operating range," *IEEE Trans. Power Electron.*, vol. 26, no. 4, pp. 1228–1236, Apr. 2011.

[8] G. G. Oggier, G. O. García, and A. R. Oliva, "Switching control strategy to minimize dual active bridge converter losses," *IEEE Trans. Power Electron.*, vol. 24, no. 7, pp. 1826–1838, Jul. 2009.

[9] A. K. Jain and R. Ayyanar, "PWM control of dual active bridge: Comprehensive analysis and experimental verification," *IEEE Trans. Power Electron.*, vol. 26, no. 4, pp. 1215–1227, Apr. 2011.

[10] F. Krismer and J. W. Kolar, "Efficiency-optimized high current dual active bridge converter for automotive applications," *IEEE Trans. Ind. Electron.*, vol. 59, no. 7, pp. 2745–2760, Jul. 2012.

[11] F. Krismer and J. W. Kolar, "Closed form solution for minimum conduction loss modulation of DAB converters," *IEEE Trans. Power Electron.*, vol. 27, no. 1, pp. 174–188, Jan. 2012.